

An efficient mixed-integer linear programming formulation for solving influence diagrams

Topias Terho^a, Fabricio Oliveira^{a,b,***}, Ahti Salo^a and Pedro Munari^c

^aDepartment of Mathematics and Systems Analysis, Aalto University, Espoo, 02150, Finland

^bDTU Management, Technical University of Denmark, , Kgs. Lyngby, 2800, Denmark

^cDepartment of Production Engineering, Federal University of São Carlos, São Carlos - SP, 13565-905, Brazil

ARTICLE INFO

Keywords:

Decision analysis
Influence diagrams
Bayesian networks
mixed-integer linear programming

ABSTRACT

Influence diagrams represent decision-making problems with interdependencies between random events, decisions, and consequences. Traditionally, they have been solved using algorithms that determine the expected utility-maximizing decision strategy. In contrast, state-of-the-art solution approaches convert influence diagrams into a mixed-integer linear programming (MILP) model, which can be solved with powerful off-the-shelf MILP solvers. From a computational standpoint, the existing MILP formulations can be efficiently solved when applied to influence diagrams that represent periodic (or sequential) decision processes, which can be cast as partially observable Markov Decision Processes. However, they are inefficient in problems that lack a periodic structure or if the nodes in the influence diagram have large state spaces, thus limiting their practical use. In this paper, we present an efficient MILP formulation that is specifically designed for influence diagrams that are challenging for the earlier MILP formulation-based methods. Additionally, we present how the proposed formulation can be adapted to maximize conditional value-at-risk and how chance and logical constraints can be incorporated into the formulation, thus retaining the modeling flexibility of the MILP-based methods. Finally, we perform computational experiments addressing problems from the literature and compare the computational efficiency of the proposed formulation against the available MILP formulations for the reported influence diagrams. We find that the MILP models based on the proposed formulations can be solved significantly more efficiently compared to the state-of-the-art when solving influence diagrams that cannot be cast as partially observable Markov decision processes.

1. Introduction

Influence diagrams (Howard and Matheson, 2005a,b) are directed graphs that represent decision problems with dependencies between uncertain events, decisions, and consequences. They are widely used to structure decision problems due to their intuitive representation of complex decision-making problems and rigorous mathematical foundations (Oni, Madson and MacKenzie, 2024; Wan, Xu, Hunt and Zhuang, 2022; Weflen, MacKenzie and Rivero, 2022; González-Ortega, Insua and Cano, 2019). Depending on the context, they have also been referred to as Bayesian decision networks (Gu, Qiu, Hu and Tang, 2024; Khosravi-Farmad and Ghaemi-Bafghi, 2020; Lu, Zhang, Hughes and Bagtzoglou, 2022; Penman, Cirulis and Marcot, 2020) or decision networks (Zhang, Qi and Poole, 1994).

In general, the solution of the underlying problem represented as an influence diagram is a decision strategy that maximizes the expected utility of consequences. There are well-established algorithms for finding the optimal

* This work was supported by the Research Council of Finland (funding decision no. 332180) and the Profi-8 project funded by the Academy of Finland (funding decision no. 365215).

** Corresponding author

✉ topias.terho@aalto.fi (T. Terho); fabricio.oliveira@aalto.fi (F. Oliveira); ahti.salo@aalto.fi (A. Salo); munari@dep.ufscar.br (P. Munari)

ORCID(s):

decision strategy. Notable examples include approaches based on node removals and arc reversals (Shachter, 1986) and dynamic programming (Tatman and Shachter, 1990). However, these algorithms can only be employed under restrictive assumptions such as perfect recall, which means that all earlier decisions and the information on which these decisions have been based are remembered when making later ones, and acyclicity, which means that the directed graph does not contain any cycles.

Perfect recall as an assumption does not hold in many real-life applications. Lauritzen and Nilsson (2001) developed the notion of a limited memory influence diagram, which relaxes this assumption. Building upon methods for influence diagrams, many well-established algorithms have been developed to find the decision strategy that maximizes expected utility in their limited memory variants. Examples include the single-value-update algorithm (Lauritzen and Nilsson, 2001), multiple-value-update (Mauá, de Campos and Zaffalon, 2012) and the k -neighborhood search algorithm (Mauá and Cozman, 2016). The developments presented in this paper apply to influence diagrams in which perfect recall is not assumed. Therefore, we use the terms influence diagram and limited memory influence diagram interchangeably.

Decision Programming (Salo, Andelman and Oliveira, 2022) and Rooted Junction Trees (RJT) (Parmentier, Cohen, Leclère, Obozinski and Salmon, 2020) are two frameworks that transform a limited memory influence diagram into a mixed-integer linear programming (MILP) model. The MILP formulations take advantage of the property that influence diagrams can be represented as piecewise multilinear mappings from the input parameters (probabilities and decisions) into outputs (expected utilities) (Borgonovo and Tonoli, 2014). An advantage of the MILP frameworks over specialized algorithms is that the resulting optimization models can be solved with efficient and ever-improving MILP solvers such as Gurobi (Gurobi Optimization, LLC, 2022). Another advantage of MILP-based frameworks is their flexibility. The optimization models can be extended to incorporate technical constraints and consider alternative risk-accounting objective functions such as conditional value-at-risk (CVaR), which represents the expected utility of consequences conditioned on the occurrence of the least preferred α -tail of the consequence distribution, α being a probability level. In contrast, the aforementioned specialized algorithms for solving influence diagrams are, to the best of our knowledge, only applicable to finding the expected utility-maximizing decision strategy.

The RJT formulation is based on a tree decomposition of the underlying influence diagram. The computational efficiency of the resulting MILP model depends on the tree decomposition that is used, which in turn depends on the structure of the underlying influence diagram. This MILP formulation performs remarkably well when applied to decision problems that can be cast as partially observable Markov Decision Processes (POMDPs); these are problems with a periodic structure. For a selected set of examples of influence diagrams that can be cast as POMDPs, we refer to the chess problem in (Parmentier et al., 2020), the classical pig-farm problem (Lauritzen and Nilsson, 2001), and the statistical process control problem (Cobb, 2021). The similarities and differences of influence diagrams and POMDPs are further discussed in Hansen (2021), who also presents a specialized algorithm that integrates the variable elimination algorithm for influence diagrams and the value iteration algorithm for POMDPs.

Recent numerical experiments have shown that the MILP formulations based on the RJT framework computationally outperform those based on the Decision Programming framework in finding the CVaR-maximizing decision strategy, and the expected utility-maximizing decision strategy subject to chance constraints (Herrala, Terho and Oliveira, 2025). To the best of our knowledge, no studies have compared the RJT framework with Decision Programming in finding pure expected utility-maximizing decision strategies. On the other hand, as demonstrated in our numerical experiments, the MILP model constructed with the RJT framework is inefficient to solve if the underlying influence diagram yields a tree with a large treewidth. This happens, for instance, if the influence diagram lacks the periodic structure of POMDPs or if the influence diagram contains nodes with a large number of possible states. We refer the reader to (Parmentier et al., 2020; Herrala et al., 2025) for a more rigorous discussion on the

size of the RJT model and its relationship to the treewidth. Being inefficient when nodes with large state spaces are present is especially problematic due to the well-documented challenges of representing continuous events in influence diagrams (Bielza, Gomez and Shenoy, 2010). There exists some work in representing continuous variables in influence diagrams, such as methods using mixtures of truncated exponentials that are easy to integrate in closed form (Cobb, 2007; Cobb and Shenoy, 2008), or Monte-Carlo sampling based method (Charnes and Shenoy, 2004). However, the resulting problems are in general extremely challenging nonlinear (and possibly large-scale) problems that can only be solved approximately. Due to these computational hurdles, the standard approach is to discretize the continuous variables. In the context of Bayesian networks and influence diagrams, discretization can be performed arbitrarily or by using specialized statistical methods (Beuzen, Marshall and Splinter, 2018). Often, the discretization is based on expert judgement (for example, see Keating, Randall, Stanton, McCormack, Lucid, Seaborn, Converse, Canessa and Moehrenschlager (2023); Mancuso, Compare, Salo and Zio (2021); de la Barra, Salo and Pourakbari-Kasmaei (2025)). In larger influence diagrams, such as Keating et al. (2023), Contasti, Firth, Baker, Brooks, Locke and Morin (2023), or in Li, Liu, Chen and Abbassi (2024), the computational limitations of the RJT formulation may force experts to settle for a coarser discretization than what is acceptable, which is likely to erode the accuracy of the solution recommendations.

Against this backdrop, this paper introduces a reformulation of the Decision Programming model, which is specifically tailored to efficiently solve influence diagrams that are difficult for the RJT framework, i.e., influence diagrams with large state spaces and a nonperiodical structure with comparatively many random variables and few decisions. This is a typical setup in many practical applications, as evidenced by numerous reported examples (Basnet, BahooToroody, Montewka, Chaal and Banda, 2023; Contasti et al., 2023; Keating et al., 2023; Khakzad, 2021; Li et al., 2024; Neuvonen, Dillon, Vilkkumaa, Salo, Jäntti and Heinävaara, 2025).

Our contributions address a key limitation of the RJT framework by introducing a MILP formulation to solve influence diagrams that are not tractable with the existing MILP formulations. Moreover, our contributions retain the modeling flexibility of the current MILP frameworks as we demonstrate how risk-aversion can be incorporated into the optimization model by employing risk-averse objective functions, such as CVaR, or by employing chance constraints. We demonstrate the computational efficiency of our reformulations by solving variants of several problems from the literature and comparing the computational times against the RJT and Decision Programming formulations. In particular, our computational experiments demonstrate that the approach based on our reformulation significantly outperforms its RJT counterpart in influence diagrams that cannot be cast as POMDPs or that have nodes associated with large state spaces. Therefore, our reformulation complements the RJT framework and advances the state-of-the-art in solving decision problems represented as influence diagrams.

The remainder of the paper is organized as follows. Section 2 presents influence diagrams and the Decision Programming-based framework. In Section 3, we develop the reformulated Decision Programming model and discuss computational aspects related to this formulation. In Section 4, we report our computational experiments. Finally, Section 5 provides conclusions and directions for further research.

2. Background

2.1. Influence Diagrams

An influence diagram $G = (N, A)$ is a directed graph consisting of nodes $N = C \cup D \cup V$ and directed arcs A connecting the nodes. Nodes are divided into three sets that represent different components of a decision problem. Chance nodes C are realizations of random events, and decision nodes D represent choices among alternatives. Finally, value nodes V represent the consequences of the decision problem. The arcs in the influence diagram represent

dependencies between the nodes. For each node $n \in N$, the information set $I(n)$ consists of the direct parents of n , i.e., the nodes from which there is an arc to n .

Chance and decision nodes have discrete and finite sets of states $S_n, n \in C \cup D$, which represent possible outcomes at chance nodes $n \in C$ or alternatives at decision nodes $n \in D$. The joint state space of a set of nodes $M \subseteq C \cup D$ is the Cartesian product $S_M = \bigtimes_{m \in M} S_m$. Moreover, the lowercase notation $s_n \in S_n$ denotes a state, i.e., an element in the state space. Similarly, $s_M = (s_m)_{m \in M}$ denotes a combination of states of the nodes contained in M . The states of nodes contained in an information set $s_{I(n)} \in S_{I(n)}$ is the *information state* of node $n \in N$.

The states of chance nodes $s_c \in S_c, c \in C$, are realizations of random variables that are characterized by a probability distribution $\mathbb{P}(s_c \mid s_{I(c)})$ that is conditional on the respective information state. These conditional probabilities are parameters in the numerical specification of the influence diagram. They can be estimated, for example, by using statistical methods or selected by eliciting expert statements (Bielza et al., 2010; Falconer, Frank, Polaschek and Joshi, 2024; French, 2024).

At decision nodes, the states $s_d \in S_d, d \in D$, represent choices among decision alternatives, whereas the information state specifies the information that is available when making the decision at d . The selected decision alternative is determined by a decision strategy $Z_d : S_{I(d)} \rightarrow S_d$. We represent the strategy as a binary variable $z(s_d \mid s_{I(d)}) \in \{0, 1\}$, such that $z(s_d \mid s_{I(d)}) = 1$ if and only if the alternative s_d is selected for the information state $s_{I(d)}$; otherwise, $z(s_d \mid s_{I(d)}) = 0$. The collection of node-specific decision strategies is denoted as $Z : \bigtimes_{d \in D} S_{I(d)} \rightarrow \bigtimes_{d \in D} S_d$. At each decision node, exactly one decision alternative per each information state is selected, i.e.,

$$\sum_{s_d \in S_d} z(s_d \mid s_{I(d)}) = 1, \forall s_{I(d)} \in S_{I(d)}. \quad (1)$$

A decision strategy is *feasible* if, in addition to (1), Z fulfills other relevant problem-specific constraints enforced on the decision strategy, such as budget limitations and logical dependencies.

The consequences associated with decisions and realizations of chance events are modeled by value nodes, which are associated with a utility function $U : S_{I(v)} \rightarrow \mathbb{R}, v \in V$ that maps the information states to a real number that represents the utility of the consequences. In case several value nodes are used, we assume that the aggregate utility is given as a sum over the node-specific utilities.

Traditionally, an influence diagram is used to find a feasible decision strategy that maximizes the expected utility of the consequences. Typically, the decision strategy is not subject to other constraints than (1). Alternatively, metrics such as CVaR can be used in place of expected utility when searching for risk-averse decision strategies.

2.2. Decision Programming

Decision programming (Salo et al., 2022) is a framework for converting an influence diagram into an MILP model. The formulation below has been proposed by Hankimaa, Herrala, Oliveira and de Balsch (2023) to improve the original MILP model with valid inequalities and reformulations.

In the Decision Programming formulation, a *path* $s = (s_n)_{n \in C \cup D}$ is a sequence of states for each chance and decision node. The set of all possible paths is denoted as $S = S_{C \cup D}$. A sequence of states $(s_m)_{m \in M}$ for a subset $M \subseteq C \cup D$ of nodes is called a *path segment*. Probability $p(s) = \prod_{c \in N^c} \mathbb{P}(s_c \mid s_{I(c)})$ represents the product of conditional probabilities of the states of the chance nodes contained in path s . Hereinafter, we use $S^> := \{s \in S \mid p(s) > 0\}$ to denote the set of those paths for which this probability is strictly greater than zero.

An *extension* of a path segment $s_M \in S_M, M \subsetneq C \cup D$ is defined as $E(s_M) := \{s' \in S \mid s'_M = s_M\}$, that is, the set of all paths that contain the segment s_M . Analogously, an extension over the paths that have a probability strictly greater than zero is denoted as $E^>(s_M) := E(s_M) \cap S^>$.

The utility associated with a path is calculated as $U(s) = \sum_{v \in V} U(s_{I(v)})$. Without loss of generality, we assume that $U(s) > 0, \forall s \in S$. Because the utilities are invariant to affine transformations and $U^>(s) = U(s) - \min_{s' \in S} \{U(s')\} + \epsilon$ with $\epsilon > 0$, can be used to derive strictly positive utilities. Both $p(s)$ and $U^>(s)$ are parameters that can be precalculated for each path $s \in S$.

The variables in the MILP are decision strategy variables $z(s_d \mid s_{I(d)}) \in \{0, 1\}, \forall d \in D, s_d \in S_d, s_{I(d)} \in S_{I(d)}$, and the *path variables* $x(s) \in \{0, 1\}, \forall s \in S^>$, which are defined as

$$x(s) = 1 \Leftrightarrow z(s_d \mid s_{I(d)}) = 1, \forall d \in D.$$

The path variables indicate which paths are active given the selected decision strategy and therefore contribute to the objective function. Specifically, we say that a path $s \in S$ is active with a decision strategy if $z(s_d \mid s_{I(d)}) = 1, \forall d \in D$, in which case $x(s) = 1$. On the other hand, if $z(s_d \mid s_{I(d)}) = 0$ for some $d \in D$, the path is not active given the decision strategy, and the path variable takes value $x(s) = 0$. Given $x(s), \forall s \in S^>$, the expected utility of strategy Z is

$$\sum_{s \in S^>} p(s)U(s)x(s). \quad (2)$$

The optimal decision strategy that maximizes expected utility can be evaluated by solving the MILP model (3)-(7)

$$\max_{z, x} \sum_{s \in S^>} p(s)U(s)x(s) \quad (3)$$

$$\text{s.t. } \sum_{s_d \in S_d} z(s_d \mid s_{I(d)}) = 1, \quad \forall d \in D, s_{I(d)} \in S_{I(d)} \quad (4)$$

$$\sum_{s \in E^>(s_d, s_{I(d)})} x(s) \leq \Gamma(s_d \mid s_{I(d)})z(s_d \mid s_{I(d)}), \quad \forall d \in D, s_d \in S_d, s_{I(d)} \in S_{I(d)} \quad (5)$$

$$z(s_d \mid s_{I(d)}) \in \{0, 1\}, \quad \forall d \in D, s_d \in S_d, s_{I(d)} \in S_{I(d)} \quad (6)$$

$$x(s) \in [0, 1], \quad \forall s \in S^>. \quad (7)$$

Constraints (4) are equivalent to (1). Constraints (5) enforce that if $z(s_d \mid s_{I(d)}) = 0$, then $x(s)$ attains value 0 for all paths $s \in E^>(s_d, s_{I(d)})$. The value $\Gamma(s_d \mid s_{I(d)})$ acts as a big-M value so that if $z(s_d \mid s_{I(d)}) = 1$, the right hand side of (5) enables all path variables $x(s)$, where $s \in E^>(s_d, s_{I(d)})$, to take value 1. Hankimaa et al. (2023) propose using $\Gamma(s_d \mid s_{I(d)})$ as

$$\Gamma(s_d \mid s_{I(d)}) = \min \left\{ |E^>(s_d, s_{I(d)})|, \frac{|E(s_d, s_{I(d)})|}{\prod_{k \in D \setminus \{d\} \cup I(d)} |S_k|} \right\}, \quad (8)$$

where $|E^>(s_d, s_{I(d)})|$ is the number of elements in the sum in the left hand side of Constraint (5) and $\frac{|E(s_d, s_{I(d)})|}{\prod_{k \in D \setminus \{d\} \cup I(d)} |S_k|}$ is an upper bound on how many path variables can be strictly greater than zero in the sum on the left hand side of Constraint (5) from decisions at decision nodes other than d . For a more rigorous explanation of the parameter $\Gamma(s_d \mid s_{I(d)})$, see Hankimaa et al. (2023). Constraints (6) and (7) define the domain of the variables.

Though the domain of path variables allows for fractional solutions, we note that the variables find the optimal solution from the set $\{0, 1\}$. This happens because the upper bound on constraint (5) is either 0 (if for any $d \in D$, $z(s_d \mid s_{I(d)}) = 0$) or $\Gamma(s_d \mid s_{I(d)})$, which is greater than or equal to 1. If $\Gamma(s_d \mid s_{I(d)})$ is the upper bound in constraints (5), constraints (7) imposes a tighter upper bound for $x(s)$. Because $U(s) > 0, \forall s \in S$, the maximization of the objective

function guides all possible $x(s)$ to take the highest possible value, which is either 0 or 1. The use of continuous path variables is further discussed in Hankimaa et al. (2023), where the authors demonstrate that continuous path variables significantly improve the computational efficiency of (3)-(7).

3. Contributions

3.1. Reformulated Decision Programming model

As Salo et al. (2022) note, the Decision Programming formulation suffers from the curse of dimensionality. The computational studies in Hankimaa et al. (2023) and Herrala et al. (2025) further show that the solution time related to the Decision Programming MILP formulation grows exponentially with respect to the number of nodes in the influence diagram. The main reason for this is the exponential growth of the number of path variables as a function of the number of chance and decision nodes. The experiments in (Hankimaa et al., 2023) also demonstrate that the LP-relaxation of (3)-(7) is weak, which significantly reduces the efficiency of MILP solvers. This motivates the development of an alternative formulation for (3)-(7) with fewer variables and a tighter formulation.

Let $C_I = \{c \in C \mid \exists d \in D \text{ s.t. } c \in I(d)\}$ and let $O = D \cup C_I$. Thus, the set O contains decision nodes and chance nodes that the decision maker observes at some point in the decision process. We call the set O as *observation set*, and a path segment s_O consisting of the states of nodes from the observation set an *observable segment*. Our reformulation is based on the following observation concerning the optimal values for path variables in (3)-(7). The observable segment s_O determines the values of path variables in the sense that if $x(s) = 1$ for some $s \in S^>$, then $x(s') = 1, \forall s' \in E^>(s_O)$. Essentially, path variables for paths with identical observation segments share the same value at the optimal solution. This is due to the fact that s_O contains all the states required to evaluate decision strategies, which ultimately determine whether $x(s) = 0$ or $x(s) = 1$. We provide a theoretical justification and demonstrate how this observation can be used to formulate an improved MILP model. Proposition 1 confirms the validity of our observation.

Proposition 1. *Let (x, z) be a feasible solution for the constraint set (4)-(7). Let x^* be such that $x^*(s) = 1$ if $\max_{s' \in E^>(s_O)} x(s') > 0$ and $x^*(s) = 0$ otherwise. Then, (x^*, z) is feasible for the constraint set (4)-(7). Moreover, if $\exists s \in S^>$ such that $x(s) \neq x^*(s)$, then $\sum_{s \in S^>} p(s)U(s)x(s) < \sum_{s \in S^>} p(s)U(s)x^*(s)$.*

Proof. See Appendix A. □

As a corollary for Proposition 1, any feasible solution (x, z) for (4)-(7) for which $\exists s, s' \in S^>$ such that $s_O = s'_O$ and $x(s) \neq x(s')$ is suboptimal. We define *observation variables* $y(s_O) \in \{0, 1\}, \forall s_O \in S_O$, with the following relationship to path variables:

$$y(s_O) = 1 \Leftrightarrow x(s) = 1, \forall s \in E^>(s_O). \quad (9)$$

Effectively, the observation variables $y(s_O)$ aggregate the path variables $x(s)$, for $s \in E^>(s_O)$ from (3)-(7). Consequently, when compared to path variables in (3)-(7), observation variables exclude solutions such that $x(s) \neq x(s')$, where $s, s' \in E^>(s_O)$, for some $s_O \in S_O$.

Let $\mathbb{E}_U(s_O) = \sum_{s \in E(s_O)} p(s)U(s)$ be the expected utility associated with an observable segment $s_O \in S_O$. Additionally, let $E_O(s_M) := \{s'_O \in S_O \mid s'_M = s_M\}$ be the *observable extension* for an observable segment $M \subseteq O$. The expected utility of the decision strategy can be represented with the observation variables as $\sum_{s_O \in S_O} \mathbb{E}_U(s_O)y(s_O)$. Proposition 2 states that $\sum_{s_O \in S_O} \mathbb{E}_U(s_O)y(s_O)$ is equal to the expected utility (2) using the path variables, as defined in (9).

Proposition 2. Let y be such that $y(s_O) \in \{0, 1\}, \forall s_O \in S_O$, and let x be defined as in (9) based on y . Then, $\sum_{s \in S_O} \mathbb{E}_U(s_O) y(s_O) = \sum_{s \in S^>} p(s) U(s) x(s)$.

Proof. See Appendix A. □

Using the results from Proposition 2, we can pose the following equivalent formulation.

$$\max_{z, y} \sum_{s_O \in S_O} \mathbb{E}_U(s_O) y(s_O) \quad (10)$$

$$\text{s.t. } \sum_{s_d \in S_d} z(s_d \mid s_{I(d)}) = 1, \quad \forall d \in D, s_{I(d)} \in S_{I(d)} \quad (11)$$

$$\sum_{s_O \in E_O(s_d, s_{I(d)})} y(s_O) \leq \Gamma(s_d \mid s_{I(d)}) z(s_d \mid s_{I(d)}), \quad \forall d \in D, s_d \in S_d, s_{I(d)} \in S_{I(d)} \quad (12)$$

$$z(s_d \mid s_{I(d)}) \in \{0, 1\}, \quad \forall d \in D, s_d \in S_d, s_{I(d)} \in S_{I(d)} \quad (13)$$

$$y(s_O) \in [0, 1], \quad \forall s_O \in S_O. \quad (14)$$

In particular, the optimal solution to (10)-(14) gives the decision strategy that maximizes expected utility. We note that Proposition 2 provides the equivalence for binary y whereas the model (10)-(14) allows y to be a continuous variable on the interval $[0, 1]$. However, with similar argumentation as in Section 2.2, we conclude that $y(s_O) \in [0, 1]$ attains the optimum value from the set $y(s_O) \in \{0, 1\}, \forall s_O \in S_O$, so that the use of continuous $y(s_O)$ is warranted. In addition, because the number of observation variables cannot exceed the number of path variables, the coefficient $\Gamma(s_d \mid s_{I(d)})$ remains a valid big-M value in Constraint (12). With Propositions 3 and 4, we show that the optimal value of (3)-(7) can be attained using the formulation (10)-(14).

Proposition 3. Let (y, z) be a solution that fulfills the constraint set (11)-(13) and (14) holds tightly (i.e. $y(s_O) \in \{0, 1\}, \forall s_O \in S_O$). Let $x^*(s) = y^*(s_O), \forall s \in S^>$. Then, (x, z) fulfills the constraint set (4)-(7).

Proof. See Appendix A. □

Proposition 4. Assume that (y^*, z^*) is the optimal solution for (10)-(14). Let $x^*(s) = y^*(s_O), \forall s \in S^>$. Then, (x^*, z^*) is the optimal solution for (3)-(7).

Proof. See Appendix A. □

Furthermore, we can strengthen formulation (10)-(14) with a valid inequality stating that for each path segment based on all chance nodes s_C , there exists at most one path s containing s_C such that $x(s) = 1$. In (10)-(14), the equivalent statement is that for each s_{C_I} , there exists at most one s_O , containing s_{C_I} such that $y(s_O) = 1$. Proposition 5 states how this can be used to generate a valid inequality for (10)-(14).

Proposition 5. Assume that (y, z) is a feasible for the constraint set (11)-(14). Then, $\sum_{s_O \in E_O(s_{C_I})} y(s_O) \leq 1, \forall s_{C_I} \in S_{C_I}$.

Proof. See Appendix A. □

Therefore, $\sum_{s_O \in E_O(s_{C_I})} y(s_O) \leq 1, \forall s_{C_I} \in S_{C_I}$, can be added to (10)-(14) to improve its LP relaxation. The final form of our proposed formulation is given in (15)-(20).

$$\max_{z, y} \sum_{s_O \in S_O} \mathbb{E}_U(s_O) y(s_O) \quad (15)$$

$$\text{s.t. } \sum_{s_d \in S_d} z(s_d | s_{I(d)}) = 1, \quad \forall d \in D, s_{I(d)} \in S_{I(d)} \quad (16)$$

$$\sum_{s_O \in E_O(s_d, s_{I(d)})} y(s_O) \leq \Gamma(s_d | s_{I(d)}) z(s_d | s_{I(d)}), \quad \forall d \in D, s_d \in S_d, s_{I(d)} \in S_{I(d)} \quad (17)$$

$$\sum_{s_O \in E_O(s_{C_I})} y(s_O) \leq 1, \quad \forall s_{C_I} \in S_{C_I} \quad (18)$$

$$z(s_d | s_{I(d)}) \in \{0, 1\}, \quad \forall d \in N^d, s_d \in S_d, s_{I(d)} \in S_{I(d)} \quad (19)$$

$$y(s_O) \in [0, 1], \quad \forall s_O \in S_O. \quad (20)$$

Remark 1. The formulation (15)-(20) can be preprocessed similarly as (3)-(7) by defining observation variables only for the observable segments, whose expected utility contribution is strictly greater than zero as $S_O^> = \{s_O \in S_O \mid \mathbb{E}_U(s_O) > 0\}$.

3.2. Alternative objective functions and risk constraints

The original formulation (3)-(7) can be easily adapted to consider alternative risk preferences to optimize risk measures like the CVaR, which is the expected value of consequences in the worst-case α -tail of the distribution, with α being a probability threshold parameter (Rockafellar, Uryasev et al., 2000). Similarly, enforcing chance constraints (Charnes and Cooper, 1959) or logical constraints is relatively straightforward. Next, we describe how the optimization model (15)-(20) can, with a suitable reformulation, be generalized to include CVaR in the objective function and to account for risk-related constraints.

3.2.1. Conditional value-at-risk

The CVaR formulation presented in Salo et al. (2022) takes advantage of the fact that the probability distribution over consequences can be represented as a function the decision variables. For instance, in (3)-(7), this is relatively straightforward as each path $s \in S$ is associated with a utility $U(s)$. Thus, the probability of attaining utility value u can be represented as $q(u) = \sum_{\{s \in S \mid U(s)=u\}} p(s)x(s)$.

In order to represent the probability distribution of consequences as variables in (15)-(20), we define the *utility extension* $E_U^u(s_O) = \{s \in E(s_O) \mid U(s) = u\}$. The utility extension for the observable segment s_O is the set of all paths containing s_O and for which the utility is u . The probability of attaining the utility u is

$$q(u) = \sum_{s_O \in S_O} y(s_O) \left(\sum_{s \in E_U^u(s_O)} p(s) \right).$$

Additionally, let us define the set $U = \{u \in \mathbb{R} \mid \exists s \in S \text{ s.t. } U(s) = u\}$. Analogous to Salo et al. (2022), we pose constraints (21)-(31).

$$\eta - u \leq M \lambda(u), \quad \forall u \in U \quad (21)$$

$$\eta - u \geq (M + \epsilon) \lambda(u) - M, \quad \forall u \in U \quad (22)$$

$$\eta - u \leq (M + \epsilon) \bar{\lambda}(u) - \epsilon, \quad \forall u \in U \quad (23)$$

$$\eta - u \geq M(\bar{\lambda}(u) - 1), \quad \forall u \in U \quad (24)$$

$$\bar{\rho}(u) \leq \bar{\lambda}(u), \quad \forall u \in U \quad (25)$$

$$q(u) - (1 - \lambda(u)) \leq \rho(u) \leq \lambda(u), \quad \forall u \in U \quad (26)$$

$$\rho(u) \leq \bar{\rho}(u) \leq q(u), \quad \forall u \in U \quad (27)$$

$$\sum_{u \in U} \bar{\rho}(u) = \alpha \quad (28)$$

$$\lambda(u), \bar{\lambda}(u) \in \{0, 1\}, \quad \forall u \in U \quad (29)$$

$$\rho(u), \bar{\rho}(u) \in [0, 1], \quad \forall u \in U \quad (30)$$

$$\eta \in \mathbb{R}. \quad (31)$$

In (21)-(31), α is the probability threshold parameter and ϵ is a small constant used to model strict inequalities. Salo et al. (2022) use $\epsilon = \frac{1}{2} \min\{|u_1 - u_2| : u_1, u_2 \in U, u_1 \neq u_2\}$, which is the smallest positive utility difference between two paths, and M is a big-M value. For a more rigorous explanation of (21)-(31), see (Salo et al., 2022; Herrala et al., 2025).

If Constraints (21)-(31) are added to (15)-(20), then CVaR is

$$\frac{1}{\alpha} \sum_{u \in U} \bar{\rho}(u)u. \quad (32)$$

This expression can be used as an alternative to the expected utility or as a constraint in the optimization model. Specifically, maximizing (32) will maximize the expected consequences in the worst α -tail of the distribution, which is equivalent to minimizing the risks associated with the worst α -tail of the consequence distribution.

The CVaR formulation (21)-(31) is based on the assumption that

$$z(s_d \mid s_{I(d)}) = 1, \forall d \in D \Leftrightarrow y(s_O) = 1, \forall s_O \in S_O \quad (33)$$

holds. That is, we assume that if all decisions in an observable segment $s_O \in S_O$ are compatible with the decision strategy, then $y(s_O) = 1$. In (15)-(20), this assumption is fulfilled implicitly by maximizing the expected utility. However, this assumption does not hold for more general objective functions. To see why, consider that in (21)-(31), the variable $\bar{\rho}(u)$ represents the *worst-case* α -tail distribution of the consequences. This is done by enforcing a lower bound on $\bar{\rho}(u)$ in Constraints (27) using another variable $\rho(u)$, which is bounded from below with expression $q(u)$, which in turn depends on $y(s_O)$. As we seek a solution where Constraint (28) holds, the lower bound $q(u)$ forces $\bar{\rho}(u)$ to attain values that are strictly positive in the worst-case tail of the probability distribution of the attainable utilities. In terms of the objective function (32), a better solution would be to set the lower bounds to zero for small utility values and seek to exhaust Constraint (28) by using paths with large utilities. Therefore, if (33) is not enforced, the model can simply set $y(s_O) = 0$ for compatible observable segments with small utility values, which sets the lower bound in Constraint (26) to zero and allows $\bar{\rho}(u)$ to seek nonzero values for large utilities. If (33) holds, then the lower bounds work as intended and $\bar{\rho}(u)$ represents the worst-case α -tail distribution. Therefore, (33) is enforced via a constraint. We do this by enforcing that Constraints (18) hold as an equality. Proposition 6 shows that enforcing Constraints (18) as equalities enforces that condition (33) holds.

Proposition 6. *Assume that (y, z) is a feasible solution for (15)-(20) where (18) holds with equality. Then, (33) holds.*

Proof. See Appendix A □

As a result, the CVaR maximizing decision strategy can be found by maximizing (32) subject to Constraints (16)-(31) and enforcing that Constraint (18) holds as an equality. For compactness, we refer to this formulation as (16)-(32). The complete model for maximizing CVaR is in Appendix B.

Remark 2. The CVaR-model cannot be preprocessed like the expected utility-maximizing model (15)-(20) by excluding observable segment $y(s_O)$ variables whose expected utility contribution is zero. Enforcing Constraints (18) as an equality will render the model infeasible if an observable segment s_O for which $\mathbb{E}_U(s_O) = 0$, is such that $z(s_d \mid s_{I(d)}) = 1, \forall d \in D$. Then, $y(s_O)$ would not be included into the model and some other path $s'_O \in E_O(s_{C_I})$ would be required to attain value $y(s'_O) = 1$ to fulfill the Constraints (18) as an equality. Based on Proposition 5, this is not possible and the model would be rendered infeasible.

3.2.2. Chance constraints

Chance constraints can be introduced to the optimization model to ensure that the probability of a state or a collection of states does not exceed a given probability threshold. In (3)-(7), chance constraints are relatively simple to impose as the set of paths S encompasses all possible state combinations of the nodes included in the influence diagrams. Let $T \subseteq C \cup D$ be the set of nodes and let $S_T \subseteq S_T$ be the set of state combinations that are subject to a chance constraint. Let $b_T \in [0, 1]$ be a probability threshold. Chance constraints can be added to (3)-(7) by introducing the constraint

$$\sum_{s \in E(s_T), s_T \in S_T} p(s)x(s) \leq b_T. \quad (34)$$

For formulation (15)-(20), the corresponding chance constraint is

$$\sum_{s_T \in S_T} \sum_{s_O \in E_O(s_{O \cap T})} y(s_O) \left(\sum_{s \in E(s_T)} p(s) \right) \leq b_T. \quad (35)$$

The set S_T and the threshold b can be adjusted to enable other types of constraints. As an example, constraints preventing budget violations should be enforced by selecting $T = \cup_{v \in \mathcal{V}} I(v)$, where $\mathcal{V} \subseteq V$ is the set of value nodes from which budget consumption is evaluated and selecting S_T to be the state combinations for which the budget would be violated. Then, enforcing Constraint (35) with $b_T = 0$ leads the model to a decision strategy that prevents budget violations. Similarly, constraints enforcing logical requirements (for example, an equipment that must be purchased in order to be utilized) can be enforced by selecting T as the nodes from which the logical requirements consist, and S_T as the joint states that violate the logical requirement. Enforcing Constraint (35) with $b_T = 0$ leads to a decision strategy that does not violate the logical requirements.

3.3. Computational considerations

Formulation (15)-(20) improves upon (3)-(7) by having fewer variables and a tighter formulation that eliminates suboptimal solutions. However, the relative performance improvement of (15)-(20) compared to (3)-(7) depends on the structure of the influence diagram. If all nodes are observed so that $O = C \cup D$, then (15)-(20) only improves upon (3)-(7) by having the additional valid inequality (18).

A key tractability bottleneck in (3)-(7) is the set of paths S , which grows exponentially with respect to the number of nodes, and their associated number of states, in the influence diagram. Although (15)-(20) does not associate a decision variable with each path, the full set of paths is still considered in the objective function. To see this, notice that the sum $\sum_{s_O \in S_O} \mathbb{E}_U(s_O)y(s_O) = \sum_{s_O \in S_O} \sum_{s \in E(s_O)} p(s)U(s)y(s_O)$ contains $|S|$ elements. On the other hand, $\mathbb{E}_U(s_O)$ is a parameter that can be precalculated for each s_O , indicating the opportunity to leverage parallel computing to reduce the preprocessing time.

4. Computational Experiments

We assess the computational performance by solving variants of reported decision-making problems with the RJT formulation, the Decision Programming formulation (3)-(7), and our proposed formulation (15)-(20). All models were implemented using Julia v1.10.3 with JuMP v1.23.0 (Lubin, Dowson, Dias Garcia, Huchette, Legat and Vielma, 2023) and solved with the Gurobi solver v11.0.2. The RJT-models and the Decision Programming formulations (15)-(20) were constructed using the Julia package DecisionProgramming.jl v2.0.1. The experiments were conducted using an Intel E5-2680 CPU at 2.5GHz with 16 GB of RAM, provided by the Aalto University School of Science “Science-IT” project. The code and data to support the numerical experiments in this section can be found via <https://github.com/toubinaattori/Decision-Programming-new-formulation>.

4.1. Assessing the optimization models

A starting point for solving an influence diagram with a MILP formulation is an influence diagram $G = (N, A)$ with discretized state spaces for the decision and chance nodes, conditional probability distributions for chance nodes, and numerical values of the utility functions at value nodes for the consequences.

Depending on the framework, an influence diagram is preprocessed differently into an MILP formulation. To build the RJT model, the influence diagram is first converted to an RJT (Parmentier et al., 2020). Then, the MILP formulation is created for G with the specified numerical parameters. To build the model (15)-(20), parameters $\mathbb{E}_U(s_O)$ are calculated for each $s_O \in S_O$. Then the corresponding MILP formulation is created with the specified numerical values. Similarly, to build the model (3)-(7), parameters $p(s)$ and $U(s)$ are calculated for each $s \in S$. The MILP formulation is created with the calculated parameters. The *preprocessing and model construction time* is denoted by τ_p . The *solution time* is denoted as τ_s .

In practice, the most important efficiency measure is the *total time*, denoted as $\tau_t = \tau_p + \tau_s$, which is the total time that is needed to formulate and solve the MILP model based on an influence diagram. Therefore, in addition to the solution time of each MILP model, we report the total time. For compactness, we do not separately report the preprocessing time, which can be recovered from the reported numerical values as $\tau_p = \tau_t - \tau_s$. We set a limit on the total time $\tau_t^{max} = 3600$ seconds. If this limit is reached, we report either the best feasible solution or that no feasible solution was found within the time limit. We denote the average total time as $\bar{\tau}_t$ and average solution time $\bar{\tau}_s$, both calculated across the sample of randomly generated instances for each problem. In cases where not all generated instances were solved to optimality within the time limit, $\bar{\tau}_t$ and $\bar{\tau}_s$ are the average times of those instances that were solved to optimality. In addition, we report the number of instances solved to optimality, denoted as “Opt (#)” and the number of instances for which a feasible solution was found within a time limit, which is denoted as “Feas (#)”. If no solutions were found within the time limit, we denote the result as “T”. In some cases, generating the MILP model required more memory than the allocated 16 GB. For these cases, we report that the cause of termination was that the processor was out of memory (OoM). Consequently, “OoM” also indicates that no feasible solutions were found for any instance of a given size.

4.2. Turbine inspection and maintenance problem

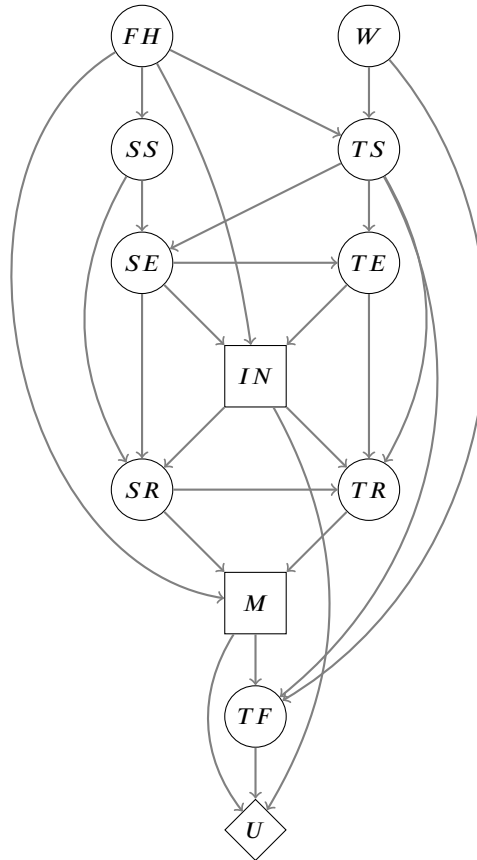
First, consider a variant of a turbine system inspection and maintenance problem in (Mancuso et al., 2021), representing a turbine and an associated sensor that are subject to wear and tear and weathering, which negatively affect the performance (i.e., the flow) of the turbine. The sensor condition and the turbine condition are both monitored by obtaining estimates, based on which a decision to carry out a more thorough inspection can be made to obtain a more accurate information about the true condition of the system. After possible inspections, the system can be maintained to increase the turbine flow. This problem is an example of an influence diagram that lacks a periodic structure and is,

Table 1

Nodes of the turbine inspection and maintenance problem

Node	Type	States	Explanation
W	Chance node	[0,100]	Turbine weathering
FH	Chance node	[0,100]	Fired hours
SS	Chance node	[0,100]	True condition of the sensor
TS	Chance node	[0,100]	True condition of the turbine
SE	Chance node	[0,100]	An estimate of the sensor condition
TE	Chance node	[0,100]	An estimate of the turbine condition
IN	Decision node	none, sensor check, turbine check	Decision to inspect the sensor and turbine
SR	Chance node	[0, 100]	Result of sensor inspection
TR	Chance node	[0, 100]	Result of turbine inspection
M	Decision node	none, level 1, level 2	Maintenance decision
TF	Chance node	[0,100]	Turbine flow after possible maintenance
U	Value node	-	Rewards minus the costs

as our numerical results corroborate, computationally demanding for the RJT framework. The nodes of the problem are listed in Table 1 and the influence diagram of the problem is in Figure 1.

**Figure 1:** Influence diagram of the turbine inspection and maintenance problem

Compared to the influence diagram used in Mancuso et al. (2021), we modify the influence diagram in three ways. In Mancuso et al. (2021), the authors assume that the node FH only has one state alternative, which consequently is known at every decision, even without having the edges (FH, IN) and (FH, M) included in the influence diagram.

In Mancuso et al. (2021), the authors then solve multiple instances of the problem with a different state for node FH . We instead solve one large influence diagram, where FH has many alternative states. Since the total of fired hours is assumed to be known at each decision node, we add the corresponding edges (FH, IN) and (FH, M) . In addition, compared to Mancuso et al. (2021), we have one additional chance node W that represents exogenous conditions that affect the state and flow of the turbine, thus making the setup more realistic.

We assume that there are three inspection alternatives (no inspection, sensor check, and turbine check) and three maintenance alternatives (no maintenance, level-1 maintenance, and level-2 maintenance) to choose from. All chance nodes in the problem represent continuous random variables. In Table 1, state 0 represents the smallest possible state for the given node. For example, $s_{FH} = 0$ represents a situation where the turbine is not running, and $s_{SS} = 0$ represents the situation where the sensor is not operational. State 100, on the other hand, represents the largest possible state. For example, $s_{FH} = 100$ represents the maximum duration that the turbine can run, and $s_{SS} = 100$ represents the situation where the sensor is in pristine condition.

An influence diagram representation of the turbine inspection and maintenance problem requires that the state spaces of chance nodes are represented as a discrete set of alternatives. We test the performance of the MILP models by solving randomly generated instances of the turbine inspection and maintenance problem when representing the state spaces of chance nodes by K different alternatives. We make minimal assumptions on the numerical parameters to create a heterogeneous set of analyzed instances. This process ensures that the resulting analyses are not dependent on assumptions about the probability distributions or consequences but give accurate insight into the effectiveness of the developed formulations.

A random instance is generated by discretizing the state spaces, generating conditional probability distributions for chance nodes, and generating the numerical output of the utility functions at the value nodes. We create the state spaces for chance nodes by randomly selecting K alternatives from the domain of the said chance node. We then create random conditional probability distributions $\mathbb{P}(s_c \mid s_{I(c)})$ for each chance node $c \in C$ and information state $s_{I(c)}$ by generating a random vector $v \in [0, 1]^K$ so that each index of v corresponds to one state $s_c \in S_c$. We then set the conditional probabilities $\mathbb{P}(s_c \mid s_{I(c)})$ to be the corresponding normalized value from v , thus guaranteeing that $\sum_{s_c \in S_c} \mathbb{P}(s_c \mid s_{I(c)}) = 1$. We randomly generate the costs of inspection alternatives by selecting two numbers from the uniform distribution $[10, 100]$ and associate the smaller cost to the sensor check and the higher cost to the turbine check. Similarly, we generate costs of maintenance decisions by selecting two random numbers from the uniform distribution $[500, 3000]$ and associate the smaller cost with the level-1 maintenance, and the higher cost with the level-2 maintenance option. The rewards associated with the turbine flow are generated by selecting K random numbers from the uniform distribution $[100, 10000]$ and sorting them so that the smallest reward is associated with the smallest turbine flow state.

We tested the computational performance of the formulations by generating and solving 50 random instances of the turbine inspection and maintenance problem with discretizations of size $K = 2, \dots, 6$ by using the proposed formulation (15)-(20), the RJT formulation, and the Decision Programming formulation (3)-(7). Table 2 presents the results of the experiments. The results show that when using the formulation (15)-(20), the solver overperforms the other models in finding the optimal solution for all generated instances, much faster compared to other formulations. In contrast, when using the RJT model, the solver is able to find the optimal solution in all generated instances of size $K = 2$. In instances of size $K \in \{3, 4\}$, when using the RJT model, the solver does not converge to the optimal solution within the time limit in all generated instances. However, a feasible solution for every instance is found. In instances of size $K \geq 5$ when using the RJT model, the solver finds no feasible solutions. In terms of total time, solution time, and the number of instances solved to optimality, using the Decision Programming formulation (3)-(7) yields the worst

Table 2

Results of the turbine monitoring and maintenance problem

K	(15)-(20)				RJT			(3)-(7)			
	$\bar{\tau}_t$ (s)	$\bar{\tau}_s$ (s)	Opt (#)	$\bar{\tau}_t$ (s)	$\bar{\tau}_s$ (s)	Opt (#)	Feas (#)	$\bar{\tau}_t$ (s)	$\bar{\tau}_s$ (s)	Opt (#)	Feas (#)
2	0.21	0.18	50/50	0.29	0.20	50/50	50/50	198.34	197.82	50/50	50/50
3	7.53	6.46	50/50	325.95	319.31	44/50	50/50	OoM	OoM	0/50	0/50
4	73.77	65.15	50/50	370.73	123.35	15/50	50/50	OoM	OoM	0/50	0/50
5	350.48	286.74	50/50	OoM	OoM	0/50	0/50	OoM	OoM	0/50	0/50
6	1457.26	1132.39	50/50	OoM	OoM	0/50	0/50	OoM	OoM	0/50	0/50

Table 3

Nodes of the extended oil wildcatter problem

Node	Type	States	Explanation
O	Chance node	dry, medium, wet	The state of the oil well
S	Chance node	dry, medium, wet	Geological features of the drilling site
T_i	Decision node	yes, no	Decision to commission test i
R_i	Chance node	N/A, dry, medium, wet	Results of test i
C_i	Value node	-	Costs of testing decision
D	Decision node	yes, no	Drilling decision
U	Value node	-	Reward minus drilling costs

performance of the solver. Significantly more time to construct the optimization model is needed, and the solver takes considerably more time to find the optimal decision strategy when compared to the other formulations. Moreover, no instances of size $K \geq 3$ are solved to optimality, which are on average solved in 7.5 seconds when using the proposed formulation (15)-(20) and in 330 seconds when using the RJT-formulation. This computational experiment showcases the value of the proposed formulation, as it enables efficiently solving instances that are intractable for existing formulations.

In addition to the computational tests presented in this section, Appendix C presents another version of the turbine inspection and maintenance problem in which we demonstrate how a specific instance of the problem with known conditional probability distributions can be discretized and solved. Moreover, we demonstrate how much the decision strategy improves using the larger state spaces with the proposed formulation (15)-(20) compared to solving the decision strategy using the largest possible state space enabled by the RJT model and the Decision Programming formulation (3)-(7), further showcasing the value of having available a more efficient formulation.

4.3. Extended oil wildcatter problem

We consider a variant of the oil wildcatter problem (Raiffa, 1968), in which a wildcatter decides whether to run a series of geological tests for a potential oil well before deciding whether or not to start drilling. In the simple version of the problem, the decision maker has only one test to choose from. More realistically, there are M tests available. Compared to the turbine inspection and maintenance problem, in the extended oil wildcatter problem, the number of nodes increases, but the number of states for each node remains constant, whereas in the turbine inspection and maintenance problem, the number of states increases, but the number of nodes remains constant. This experiment provides insight into how the formulation (15)-(20) performs computationally in comparison with the current state-of-the-art for influence diagrams with multiple nodes having fewer state alternatives (i.e., smaller state spaces in each node). The influence diagram of the extended oil wildcatter problem with two tests is illustrated in Figure 2 with its nodes described in Table 3.

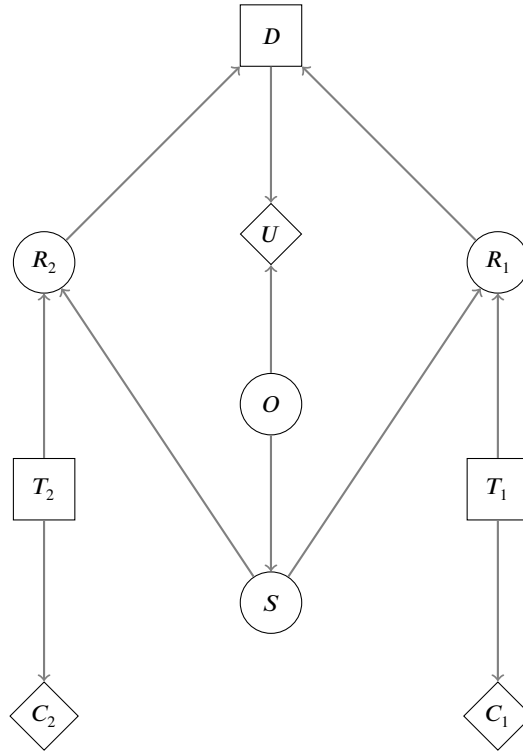


Figure 2: Influence diagram of the extended oil wildcatter problem, where $M = 2$

We create random instances of the extended oil wildcatter problem by randomly generating conditional probabilities and utilities. We created random conditional probabilities for each chance node similarly as in the turbine inspection and maintenance problem by enforcing that $\sum_{s_c \in S_c} \mathbb{P}(s_c \mid s_{I(c)}) = 1, \forall c \in C, s_{I(c)} \in S_{I(c)}$. For nodes R_i that represent reports on tests, the conditional probabilities are such that $\mathbb{P}(s_{R_i} = N/A \mid s_{T_i} = \text{yes}) = 0$ and $\mathbb{P}(s_{R_i} = N/A \mid s_{T_i} = \text{no}) = 1$. The utilities are generated by randomly selecting a cost for each test from the uniform distribution [1, 50] and the drilling costs from the uniform distribution [50, 90]. Payoffs are generated by selecting two random numbers from the uniform distribution [100, 1000] and ordering them so that $s_O = \text{medium}$ is associated with the smaller payoff and $s_O = \text{wet}$ is associated with the larger payoff. The state $s_O = \text{dry}$ is associated with zero payoff. Moreover, if $s_D = \text{no}$, drilling is not started and the payoff will be zero. The utility at U is calculated by subtracting the testing and building costs from the payoffs.

For each $M = 2, \dots, 8$, we generated and solve 50 random instances. We report the number of instances solved to optimality, the number of instances for which a feasible solution was found, the average total times, and average solution times of the solved instances in Table 4.

The results show that the formulation (15)-(20) dominates the other formulations in terms of total time, solution time, and solution quality. The total times are on average 1-2 orders of magnitude smaller when using (15)-(20) to find the optimal decision strategy compared to using the RJT model or (3)-(7). Additionally, when using (15)-(20), all evaluated instances converge to the optimal solution. When using the RJT model, the solver runs out of memory to generate any of the instances of size $M \geq 7$. Similarly, no feasible solutions for problem instances of size $M \geq 7$ can be found using (3)-(7).

The computational experiments on the extended oil wildcatter problem indicate that the proposed formulation results in significant computational improvements in solving problems that contain many nodes and few states at chance

Table 4

Results of the extended oil wildcatter problem

M	(15)-(20)			RJT			(3)-(7)				
	$\bar{\tau}_t$ (s)	$\bar{\tau}_s$ (s)	Opt (#)	$\bar{\tau}_t$ (s)	$\bar{\tau}_s$ (s)	Opt (#)	Feas (#)	$\bar{\tau}_t$ (s)	$\bar{\tau}_s$ (s)	Opt (#)	Feas (#)
1	0.02	0.0010	50/50	0.22	0.0021	50/50	50/50	0.12	0.003	50/50	50/50
2	0.02	0.0012	50/50	0.28	0.0055	50/50	50/50	0.15	0.027	50/50	50/50
3	0.02	0.0016	50/50	0.63	0.027	50/50	50/50	0.37	0.067	50/50	50/50
4	0.05	0.0049	50/50	4.22	0.11	50/50	50/50	2.24	0.55	50/50	50/50
5	0.37	0.044	50/50	57.73	0.79	50/50	50/50	21.53	2.14	50/50	50/50
6	5.14	2.73	50/50	1330.76	5.35	50/50	50/50	308.31	5.92	50/50	50/50
7	25.24	8.11	50/50	OoM	OoM	0/50	0/50	T	T	0/50	0/50
8	332.41	55.94	50/50	OoM	OoM	0/50	0/50	OoM	OoM	0/50	0/50

Table 5

Nodes of the risk-averse water management problem

Node	Type	States	Explanation
A	Chance node	[0,100]	Agriculture activity
W_1	Chance node	[0,100]	Water quality before dilution
W_2	Chance node	[0,100]	Water quality after dilution
F	Chance node	[0,100]	Forecast of water quality
M	Decision node	level 1, level 2, level 3	Water quality monitoring strategy
D	Decision node	[0,100]	Amount of clean water admitted into the lake
C	Chance node	[0,100]	Cost of dilution
V	Value node	-	Rewards minus monitoring and dilution costs

and decision nodes. Although the solution times improve drastically when using (15)-(20), the solution times still grow exponentially as a function of the number of nodes in the influence diagram.

4.4. Risk-averse water management problem

As the final computational example, we consider a variant of the environmental management problem for the restoration of the Tuusulanjärvi lake reported by Varis, Kettunen and Sirviö (1990). The problem consists of deciding on a monitoring strategy to track and a dilution strategy to improve the water quality of the lake. Compared to the influence diagram presented in Varis et al. (1990), we have an additional chance node A that represents exogenous agricultural activity that affects the water quality of the lake. The influence diagram of the problem is in Figure 3, and the nodes are in Table 5. As in the turbine inspection and maintenance problem, the nodes with inherently continuous states are represented with states lying within the interval $[0,100]$, where 0 is the smallest possible value, and 100 represents the largest possible value. For example, $s_A = 100$ represents the highest possible agricultural activity, which produces the largest considered amount of excess fertilizers, which leads to lower water quality. For the water quality before and after dilution, $s_{W_i} = 100$ represents the best possible quality and $s_{W_i} = 0$ represents the worst possible quality. For each problem instance, we select K discrete states from the domain of continuous variables.

We created problem instances by generating random probabilities such that $\sum_{s_c \in S_c} \mathbb{P}(s_c \mid s_{I(c)}) = 1, \forall c \in C, s_{I(c)} \in S_{I(c)}$. The utilities are generated so that, for the costs of the monitoring strategy, we generate three random numbers from the uniform distribution $[0, 100]$ and associate the largest value with level-3 monitoring and the smallest value with level-1 monitoring. The state s_C represents the dilution cost. For the reward for posterior water quality, we generate K random numbers from the uniform distribution $[0, 500]$ and sort these in increasing order so that the best posterior water quality state is associated with the largest reward.

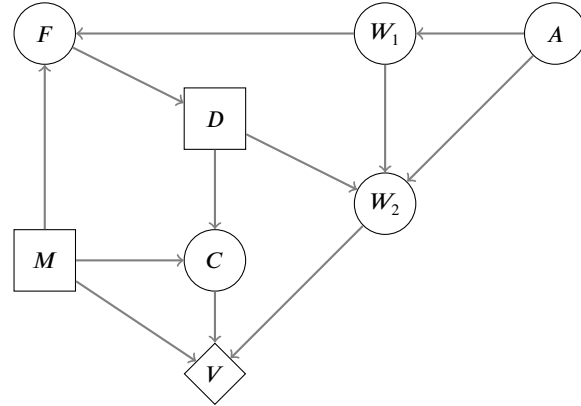


Figure 3: Influence diagram of the risk-averse water resource management problem

Table 6

Results of the risk-averse water management problem

K	(16)-(32)			RJT				DP-CVaR			
	$\bar{\tau}_t$ (s)	$\bar{\tau}_s$ (s)	Opt (#)	$\bar{\tau}_t$ (s)	$\bar{\tau}_s$ (s)	Opt (#)	Feas (#)	$\bar{\tau}_t$ (s)	$\bar{\tau}_s$ (s)	Opt (#)	Feas (#)
2	0.06	0.04	50/50	0.04	0.02	50/50	50/50	0.36	0.18	50/50	50/50
3	0.06	0.04	50/50	0.28	0.12	50/50	50/50	28.63	27.96	50/50	50/50
4	0.10	0.07	50/50	1.94	0.65	50/50	50/50	1068.33	1064.70	50/50	50/50
5	0.21	0.18	50/50	12.57	3.47	50/50	50/50	T	T	0/50	48/50
6	0.43	0.39	50/50	71.64	16.18	50/50	50/50	T	T	0/50	41/50
7	0.89	0.83	50/50	297.78	37.64	50/50	50/50	T	T	0/50	10/50
8	1.23	1.11	50/50	1032.05	106.58	50/50	50/50	OoM	OoM	0/50	0/50
9	3.18	2.95	50/50	3462.71	1134.74	33/50	36/50	OoM	OoM	0/50	0/50
10	3.91	3.43	50/50	OoM	OoM	0/50	0/50	OoM	OoM	0/50	0/50

In contrast to the examples in Sections 4.2 and 4.3 where influence diagrams were solved by maximizing the expected utility, we use (16)-(32) to find the strategy that minimizes risks by maximizing the CVaR given a probability threshold $\alpha = 0.2$, which implies a confidence level of 80%. We compare solution times by solving the same instances with the CVaR formulation of the RJT framework presented in Herrala et al. (2025) and with the CVaR formulation for Decision Programming, which uses the optimization model presented in Hankimaa et al. (2023) with constraints (21)-(31) and the objective function defined as in (32). We refer to this model as DP-CVaR.

We report the results of 50 randomly generated instances for values of K between 2 and 10 in Table 6. They show that using (16)-(32) significantly improves the computational time needed for finding the CVaR maximizing strategy. The total times required for solving (16)-(32) are significantly better in instances of size $K \geq 3$, and the difference becomes more pronounced for larger instances. Similarly, (16)-(32) can be solved faster than the RJT and DP-CVaR models in instances of size $K \geq 3$. In terms of solution optimality when using the RJT model, the solver only finds optimal solutions in 33 instances of size $K = 9$ and a feasible solution in only 36 instances of the same size. In instances of size $K = 10$ when using the RJT framework, the solver finds no feasible solutions, whereas when using (16)-(32) the solver takes on average less than 4 seconds to find the optimal solution. When using the DP-CVaR model, the solver does not find any optimal solutions for instances of size $K \geq 5$, and it fails to find any feasible solutions for instances of size $K \geq 8$.

Taken together, these computational experiments show that (16)-(32) significantly improves the efficiency in finding the CVaR maximizing decision strategy. Instances that have been intractable for the existing formulations

can be solved to optimality in a few seconds using (16)-(32). In addition, the total time for (16)-(32) does not grow exponentially, suggesting that considerably larger instances of the risk-averse water resource management problem can be solved to optimality within a reasonable time with the proposed formulation.

5. Conclusions

In this paper, we propose a novel MILP formulation for Decision Programming that builds upon that originally presented in (Salo et al., 2022). The proposed formulation improves the existing formulation by aggregating decision variables, which results in an MILP formulation that can be solved more efficiently. We rigorously demonstrate how this aggregation can be performed while retaining the validity of the model. Moreover, we improve the resulting MILP formulation by introducing a valid inequality.

In addition to maximizing expected utility, we present how our formulation can be generalized to optimize CVaR and how chance constraints can be imposed on the optimization model. We demonstrate the computational efficiency of the proposed formulations by solving variants of problems from the literature and compare the solution times to the RJT framework (Parmentier et al., 2020; Herrala et al., 2025), and to the Decision Programming formulation presented in (Hankimaa et al., 2023), which, to the best of our knowledge, comprise the state-of-the-art MILP formulations for decision-making problems represented by influence diagrams. We find that the MILP models based on the proposed formulations are significantly more efficient to solve compared to the MILP models based on the existing frameworks across all analyzed problem types.

Our main contribution lies in computational improvements. As our experiments demonstrate, the RJT framework struggles when the problem lacks a periodic structure or if the influence diagram contains nodes with large state spaces. The proposed formulation is designed to address such problems efficiently and, therefore, can be seen as a complement to the RJT framework. Ultimately, our formulation helps solve influence diagrams that previously have not been tractable. Our developments are especially valuable in permitting finer state-space discretizations when solving influence diagrams in which either decision or chance nodes represent decisions or random variables that are measured on continuous scales.

Despite the improvements, the presented reformulation is still subject to the computational issues related to solving influence diagrams using MILP formulations. In particular, the computational efficiency of the presented formulations depends on the structure of the influence diagram. For instance, influence diagrams that lack a periodic structure and contain relatively many decision nodes and relatively few chance nodes are typically challenging to solve with both the RJT framework and the formulations presented in this paper. In addition, the proposed formulation still exhibits exponential growth with respect to the number of nodes in the observation set, which limits the size of the influence diagrams that can be solved. Thus, future research should then focus on these drawbacks by developing new MILP formulations that can be solved more efficiently, in particular, exploring possible valid inequalities and specialized solution algorithms for the MILP models, such as decomposition approaches.

Our developments were originally inspired by the discussion in (Salo et al., 2022), who pointed to the possibility of aggregating the information needed for defining optimal decisions as a direction for development. In light of the effectiveness of the proposed reformulation, we believe that this is still a valuable future research direction, i.e., to explore other means of variable aggregations to reduce the scale of the resulting formulation even further. Moreover, a rigorous analytical framework for choosing the most effective MILP model when solving an influence diagram is yet to be developed. Therefore, future research efforts should be directed toward finding effective heuristics or statistical guarantees that would guide the selection of the framework to solve a given influence diagram as efficiently as possible.

A. Proofs

Proof of Proposition 1

First, we show that (x^*, z) fulfills constraints (4)-(7). Because (x, z) is assumed to fulfill the constraints (4)-(7), Constraints (4) are trivially fulfilled by (x^*, z) . Similarly, Constraints (6) and (7) are trivially fulfilled. Then, it remains to show that (x^*, z) fulfills Constraint (5).

Consider $s \in S^>$. If $x^*(s) = 0$, Constraints (5) are trivially fulfilled. If $x^*(s) = 1$, then there must exist $s' \in E(s_O)$ such that $x(s') > 0$. As we assume (x, z) to be feasible for (4)-(7), it necessarily follows that $z(s'_d \mid s'_{I(d)}) = 1, \forall d \in D$, where s'_d and $s'_{I(d)}$ are taken from s' . Also note that $d \in O$ and $I(d) \subsetneq O, \forall d \in D$. Moreover, as we assume that $s' \in E(s_O)$, we have that $s_O = s'_O$. Therefore it follows that $z(s'_d \mid s'_{I(d)}) = z(s_d \mid s_{I(d)}) = 1, \forall d \in D$, where s_d and $s_{I(d)}$ are taken from s . Hence, Constraint (5) is also fulfilled, and (x^*, z) is feasible for (4)-(7).

Next, we prove the suboptimality of (x, z) . Notice that in (4)-(7) we assume $U(s) > 0, \forall s \in S^> \supseteq S$ and $p(s) > 0, \forall s \in S^>$. As we assume that $x^*(s) = \max_{s' \in E^>(s_O)} x(s')$, we have that $x^*(s) \geq x(s), \forall s \in S^>$. Therefore, it follows that $p(s)U(s)x^*(s) \geq p(s)U(s)x(s), \forall s \in S^>$. Moreover, by assumption that $\exists s \in S^>$ s.t. $x(s) \neq x^*(s)$ there exists at least one $s \in S^>$ such that $x^*(s) > x(s)$. Then, $\sum_{s \in S^>} p(s)U(s)x^*(s) > \sum_{s \in S^>} p(s)U(s)x(s)$ follows.

Proof of Proposition 2

Notice the following:

$$\begin{aligned} \sum_{s \in S_O} \mathbb{E}_U(s_O) y(s_O) &= \sum_{s \in S_O} \left[\sum_{s' \in E(s_O)} p(s')U(s') \right] y(s_O) = \sum_{s \in S_O} \sum_{s' \in E(s_O)} p(s')U(s')y(s_O) = \\ &= \sum_{s \in S_O} \left[\sum_{s' \in E(s_O) \setminus S^>} p(s')U(s')y(s_O) + \sum_{s' \in E^>(s_O)} p(s')U(s')y(s_O) \right] = \\ &= \sum_{s \in S_O} \sum_{s' \in E^>(s_O)} p(s')U(s')y(s_O) = \sum_{s \in S_O} \left[\sum_{s' \in E^>(s_O)} p(s')U(s')x(s') \right] = \\ &= \sum_{s \in S^>} p(s)U(s)x(s). \end{aligned}$$

The first equality follows directly from the definition of $\mathbb{E}_U(s_O)$. The second equality simply moves $y(s_O)$ inside the inner sum. The third equality splits the inner sum. The fourth equality follows from the definition of $S^>$ so that $p(s') = 0, \forall s' \in E(s_O) \setminus S^>$. The fifth equality follows based on (9), which reduces to $x(s') = y(s_O), \forall s' \in E(s_O)$. The last equality simply combines the sums.

Proof of Proposition 3

Assume that (y, z) is a feasible solution for (11)-(14). Constraints (11) and (4) are equivalent, and therefore, by assumption $z(s_d \mid s_{I(d)})$ fulfills (4). Additionally, Constraints (6) and (7) hold trivially.

Let $d \in D$, $s_d \in S_d$, and $s_{I(d)} \in S_{I(d)}$. For Constraints (5), assume that $y(s_O) = 1$ for some $s_O \in E_O(s_{\{d\} \cup I(d)})$. Then, according to constraints (12), $z(s_d \mid s_{I(d)}) = 1$. Then, the corresponding Constraints (5) for d, s_d , and $s_{I(d)}$ reduce to

$$\sum_{s \in E(s_{\{d\} \cup I(d)})} x(s) \leq \Gamma(s_d \mid s_{I(d)}).$$

According to (9), $x(s) = 1, \forall s \in E(s_O)$. As we assume $s_O \in E_O(s_{\{d\} \cup I(d)})$, it also means that $s \in E(s_{\{d\} \cup I(d)})$, $\forall s \in E(s_O)$. As we assume $\Gamma(s_d \mid s_{I(d)})$ to be a bigM-constant for (3)-(7), $x(s) = 1, \forall s \in E(s_O)$ is a feasible solution. Conversely, assume that $y(s_O) = 0$ for some s_O . Then, $x(s) = 0, \forall s \in E(s_O)$. Then, Constraints (5) are trivially fulfilled for any feasible $z(s_d \mid s_{I(d)})$.

Proof of Proposition 4

Assume that (y^*, z^*) is an optimal solution for (10)-(14). First, due to Proposition 3, (x^*, z^*) is a feasible solution that fulfills the constraint set (4)-(7). By an optimality argument, it follows that for any (y, z) , which is feasible for (10)-(14), we have that

$$\sum_{s_O \in S_O} \mathbb{E}_U(s_O) y(s_O) \leq \sum_{s_O \in S_O} \mathbb{E}_U(s_O) y^*(s_O).$$

Let (x, z) be a feasible solution for the constraint set (4)-(7). Let $x'(s) = \max_{s' \in E(s_O)} x(s')$. Then, the following holds true:

$$\begin{aligned} \sum_{s \in S^>} p(s) U(s) x(s) &\leq \sum_{s \in S^>} p(s) U(s) x'(s) = \sum_{s \in S} p(s) U(s) x'(s) = \sum_{s_O \in S_O} \mathbb{E}_U(s_O) y'(s_O) \leq \\ \sum_{s_O \in S_O} \mathbb{E}_U(s_O) y^*(s_O) &= \sum_{s \in S^>} p(s) U(s) x^*(s). \end{aligned}$$

Notice that if $x(s) = 1$ for any $s \in S^>$, then $x'(s') = 1, \forall s' \in E(s_O)$ and therefore, x' can be represented with y' as defined in (9) based on x' without loss of generality. The first inequality follows from the assumption that $p(s)U(s) \geq 0, \forall s \in S$ and the assumption that $x'(s) \geq x(s), \forall s \in S$. The first equality holds due to adding terms for paths $s \in S \setminus S^>$, for which $p(s) = 0$. The second equality follows from Proposition (2). The second inequality follows from the assumption of optimality of y^* and the last equality follows by applying Proposition 2 and transformation (9). Therefore, (x^*, z^*) is optimal for (3)-(7).

Proof of Proposition 5

Consider $\bar{s}_{C_I} \in S_{C_I}$ and $s_O, s'_O \in E_O(\bar{s}_{C_I})$ so that $s_O \neq s'_O$. Then, $\exists d \in D$ s.t. $s_d \neq s'_d$. Assume that $y(s_O) = 1$. The assumption $y(s_O) = 1$ implies that $z(s_d \mid s_{I(d)}) = 1$ for all $d \in D$, where s_d and $s_{I(d)}$ are extracted from s_O . To prove the claim, we will show that there must exist $d \in D$ such that $z(s'_d \mid s'_{I(d)}) = 0$, where s'_d and $s'_{I(d)}$ are extracted from s'_O . If this is the case, Constraints (12) ensure that $y(s'_O) = 1$ is not a feasible solution for constraint set (10)-(14).

Denote $I_C(d) = C \cap I(d)$ and $I_D(d) = D \cap I(d)$ as the chance nodes and decision nodes contained in an information set of $d \in D$. Since we assume that value nodes cannot be parents of other nodes, $I(d) = I_C(d) \cup I_D(d)$. By assumption, $\exists d \in D$ such that $s'_d \neq s_d$. If $I_D(s_d) = \emptyset$, it means that $z(s'_d \mid s'_{I(d)}) = 0$. To see this, note that $I_C(d) \subseteq C_I$ and subsequently $s'_{I_C(d)} = s_{I_C(d)}$. Consequently $s_{I(d)} = s'_{I(d)}$. By assumption of $y(s_O) = 1$, it holds that $z(s_d \mid s_{I(d)}) = 1$. Constraints (11) then force $z(s'_d \mid s_{I(d)}) = 0$. Then, according to (12), $y(s'_O)$ would be forced to take value 0.

If $z(s'_d \mid s'_{I(d)}) = 1$, it then necessarily means that $I_D(d) \neq \emptyset$ and $\exists d' \in I_D(d)$ such that $s'_{d'} \neq s_{d'}$. A similar inspection shows that if $z(s'_{d'} \mid s'_{I(d')}) = 1$, it then follows that $I_D(d') \neq \emptyset$ and $\exists d'' \in I_D(d')$ such that $s'_{d''} \neq s_{d''}$. As the influence diagram is assumed to be acyclic, this process must eventually find d^* such that $s_{d^*} \neq s'_{d^*}$ and $I_D(d^*) = \emptyset$. Then, by assumption and Constraint (11), $z(s'_{d^*} \mid s'_{I(d^*)}) = 0$ and consequently, $y(s'_O) = 0$.

Proof of Proposition 6

We will prove the claim by using a contradiction. Assume that (y, z) is a feasible solution for (15)-(20) where (18) are equality constraints. Denote $I_C(d) = C \cap I(d)$ and $I_D(d) = D \cap I(d)$ as the chance nodes and decision nodes

contained in an information set of $d \in D$. Assume that $\exists s_O \in S_O$ such that $z(s_d | s_{I(d)}) = 1, \forall d \in D$ and assume that $y(s_O) = 0$. This would contradict (33). Then, based on Constraints (18), $\exists s'_O \in E_O(s_{C_I})$ such that $y(s'_O) = 1$, where s_{C_I} is constructed with states from s_O . Next, we will prove that $\exists d \in D$ is such that $z(s'_d | s'_{I(d)}) = 0$, which would make $y(s'_O) = 1$ infeasible.

By assumption $s'_O \neq s_O$ and $s'_{C_I} = s_{C_I}$. Then necessarily $\exists d \in D$ such that $s'_d \neq s_d$. If $I_D(d) = \emptyset$, it means that $z(s'_d | s'_{I(d)}) = 0$. To see this, note that $s'_{I(d)} = s_{I(d)}$, and consequently $s_{I(d)} = s'_{I(d)}$. As we assume $z(s_d | s_{I(d)}) = 1$, Constraints (11) then force $z(s'_d | s_{I(d)}) = 0$. Then, according to constraint (12), $y(s'_O)$ would be forced to take value 0, which would then be a contradiction.

If $z(s'_d | s'_{I(d)}) = 1$, it then necessarily means that $I_D(d) \neq \emptyset$ and $\exists d' \in I_D(d)$ such that $s'_{d'} \neq s_{d'}$. A similar inspection shows that if $z(s'_{d'} | s'_{I(d')}) = 1$, it then follows that $I_D(d') \neq \emptyset$ and $\exists d'' \in I_D(d')$ such that $s'_{d''} \neq s_{d''}$. As the influence diagram is assumed to be acyclic, this process must eventually find d^* such that $s_{d^*} \neq s'_{d^*}$ and $I_D(d^*) = \emptyset$. Then, by assumption and Constraints (11), $z(s'_{d^*} | s'_{I(d^*)}) = 0$ and consequently, $y(s'_O) = 0$. This shows that $y(s'_O) = 0, \forall s'_O \in E_O(s_I) \setminus \{s_O\}$. Then, the only way to fulfill Constraints (18) is to have $y(s_O) = 1$, which proves the claim.

B. Conditional value-at-risk model

The optimization model (36)-(52) leads to the decision strategy that maximizes CVaR at probability level α .

$$\max_{\substack{z, y, \rho, \bar{\rho}, \\ \eta, \lambda, \bar{\lambda}}} \frac{1}{\alpha} \sum_{u \in U} \bar{\rho}(u) u \quad (36)$$

$$\text{s.t. } \sum_{s_d \in S_d} z(s_d | s_{I(d)}) = 1, \quad \forall d \in D, s_{I(d)} \in S_{I(d)} \quad (37)$$

$$\sum_{s_O \in E_O(s_d, s_{I(d)})} y(s_O) \leq \Gamma(s_d | s_{I(d)}) z(s_d | s_{I(d)}), \quad \forall d \in D, s_d \in S_d, s_{I(d)} \in S_{I(d)} \quad (38)$$

$$\sum_{s_O \in E_O(s_{C_I})} y(s_O) = 1, \quad \forall s_{C_I} \in S_{C_I} \quad (39)$$

$$\eta - u \leq M \lambda(u), \quad \forall u \in U \quad (40)$$

$$\eta - u \geq (M + \epsilon) \lambda(u) - M, \quad \forall u \in U \quad (41)$$

$$\eta - u \leq (M + \epsilon) \bar{\lambda}(u) - \epsilon, \quad \forall u \in U \quad (42)$$

$$\eta - u \geq M(\bar{\lambda}(u) - 1), \quad \forall u \in U \quad (43)$$

$$\bar{\rho}(u) \leq \bar{\lambda}(u), \quad \forall u \in U \quad (44)$$

$$q(u) - (1 - \lambda(u)) \leq \rho(u) \leq \lambda(u), \quad \forall u \in U \quad (45)$$

$$\rho(u) \leq \bar{\rho}(u) \leq q(u), \quad \forall u \in U \quad (46)$$

$$\sum_{u \in U} \bar{\rho}(u) = \alpha \quad (47)$$

$$\lambda(u), \bar{\lambda}(u) \in \{0, 1\}, \quad \forall u \in U \quad (48)$$

$$y(s_O) \in [0, 1], \quad \forall s_O \in S_O \quad (49)$$

$$z(s_d | s_{I(d)}) \in \{0, 1\}, \quad \forall d \in D, s_d \in S_d, s_{I(d)} \in S_{I(d)} \quad (50)$$

$$\rho(u), \bar{\rho}(u) \in [0, 1], \quad \forall u \in U \quad (51)$$

Table 7

Conditional probability distributions for chance nodes

Node	Information set	States	PDF
FH	—	—	$\mathcal{U}(0, 100)$
W	—	—	$\mathcal{U}(0, 100)$
SS	FH	—	$\mathcal{N}(100 - s_{FH}, [10, 100])$
TS	FH, W	—	$\mathcal{N}(100 - (s_{FH} + s_W)/2, [10, 100])$
SE	SS, TS	—	$\frac{s_{TS}}{100} \mathcal{N}(s_{SS}, [10, 100]) + \frac{100-s_{TS}}{100} \mathcal{U}(0, 100)$
TE	TS, SE	—	$\mathcal{N}(s_{SS}, \frac{100-s_{SE}}{5})$
SR	I, SS, SE	$\begin{array}{l} s_I = 0 \\ s_I \in \{1, 2\} \end{array}$	$\begin{array}{l} \delta(s_{SE}) \\ \mathcal{N}(s_{SS}, 1) \end{array}$
TR	I, TS, TE, SR	$\begin{array}{l} s_I = 0 \\ s_I = 1 \\ s_I = 2 \end{array}$	$\begin{array}{l} \delta(s_{TE}) \\ \frac{s_{SR}}{100} \mathcal{N}(s_{TS}, [0.2, 10]) + \frac{100-s_{SR}}{100} \mathcal{U}(0, 100), \\ \mathcal{N}(s_{TS}, [0.2, 10]) \end{array}$
TF	M, TS, W	$\begin{array}{l} s_M = 0 \\ s_M = 1 \\ s_M = 2 \end{array}$	$\begin{array}{l} \mathcal{N}_{(0, s_{TS})}(s_{TS} - 0.02s_W, [0.2, 10]) \\ \mathcal{N}_{(s_{TS}, 100)}(s_{TS} + \frac{(100-s_{TS})}{2} - 0.02s_W, [0.2, 10]) \\ \mathcal{N}_{(s_{TS}, 100)}(100, [0.2, 10]) \end{array}$

$$\eta \in \mathbb{R}. \quad (52)$$

C. Continuous turbine inspection and maintenance problem

Consider the turbine inspection and maintenance problem presented in Section 4.2. We now assume that the chance nodes described in Table 1 are associated with continuous probability distributions that are specified in Table 7. We denote $\mathcal{N}(\mu, [\sigma_1^2, \sigma_2^2])$ a normal distribution with mean μ and a randomly generated variance $\sigma^2 \in [\sigma_1^2, \sigma_2^2]$ truncated on interval $[0, 100]$. We denote as $\mathcal{N}_{(a,b)}(\mu, [\sigma_1^2, \sigma_2^2])$ as the normal distribution with mean μ and random variance σ^2 truncated on interval $[a, b]$. We denote by $\delta(a)$ the Dirac delta distribution on a . Finally, we denote $\mathcal{U}(a, b)$ as the uniform distribution on the interval $[a, b]$. Table 7 presents the assumed conditional probability distributions. In the table, the column *States* specifies the condition that the information state must fulfill for the probability distribution to be as specified. For instance, the conditional probability distribution for node TR is $\delta(s_{TE})$ if $s_I = 0$, meaning that if no inspection is conducted, then the probability distribution of the turbine inspection result -node will assign all probability mass on the turbine state estimate. For TR , the variances are randomly generated by selecting two values from the uniform distribution $[0.2, 10]$ and associating the larger variance with the probability distribution conditional on $s_I = 1$. Similarly, we generate the variances for TF by randomly selecting three numbers from the uniform distribution $[0.2, 10]$ and associating the largest variance with the probability distribution conditional on $s_M = 0$ and the smallest variance with $s_M = 2$.

We create random instances of the turbine inspection and maintenance problem by randomly selecting the variances for the continuous probability distributions of the chance nodes. We specify the domains for possible variance values in Table 7, which are uniformly sampled to create continuous probability distributions for the chance nodes. Moreover, we

Table 8

Breakpoints used in the turbine inspection and maintenance problem

N	b_n
2	50
3	50, 75
4	25, 50, 75
5	25, 50, 75, 87.5
6	25, 50, 62.5, 75, 87.5

randomly generate the costs of the maintenance and inspection alternatives. The cost of the sensor check is uniformly sampled from $[0, 20]$, the cost of turbine inspection is uniformly sampled from $[50, 300]$, the cost of level-1 maintenance is uniformly sampled from $[100, 2000]$, and finally, the cost of level-2 maintenance is uniformly sampled $[3000, 8000]$. We assume that the turbine flow results in rewards given by the function $f(s_{TF}) = \frac{1}{100}s_{TF}^3$. The utility associated with consequences is calculated by subtracting maintenance and inspection costs from turbine flow rewards.

The influence diagram representation of the turbine inspection and maintenance problem requires the continuous events to be discretized and represented as a finite set of possible states. To create a discretization of size N , we select $N - 1$ breakpoints $b_n, n \in 1, \dots, N - 1$, from the domain of the continuous state space of each chance node $c \in C$. We create the discrete state space as $S_c = \{[0, b_1], [b_1, b_2], \dots, [b_n, 100]\}$. Table 8 presents the breakpoints used in this computational example. For simplicity, we use the same set of breakpoints for each chance node. We create conditional probabilities by generating a set of sample paths \bar{S} by sampling the conditional probability distributions presented in Appendix C. From the sample paths, we derive discrete conditional probabilities as $\mathbb{P}(s_c \mid s_{I(c)}) = |\{\bar{s} \in \bar{S} : \bar{s}_c \in s_c, \bar{s}_{I(c)} \in s_{I(c)}\}| / |\{\bar{s} \in \bar{S} : \bar{s}_{I(c)} \in s_{I(c)}\}|$. Utilities $U(s_{I(v)})$ are created by calculating the average utility for sample paths that have the states $s_{I(v)}$ as $U(s_{I(v)}) = \sum_{s \in \bar{S}_{s_{I(v)}}} \frac{U(s)}{|\bar{S}_{s_{I(v)}}|}$, where $\bar{S}_{s_{I(v)}} = \{\bar{s} \in \bar{S} : \bar{s}_{I(v)} \in s_{I(v)}\}$.

To then highlight the value of the proposed formulation, we compare the performance of the decision strategies generated using discretizations of size $N = 2, \dots, 6$, when applied to the turbine inspection and maintenance problem. We randomly generate 400 continuous instances of the problem and solve the optimal decision strategies using discretizations based on the breakpoints specified in Table 8 with the discretization method described in this section. In each of the 400 analyzed instances, we test the derived decision strategies by sampling 100 000 paths in which we separately apply the decision strategies derived by using different discretizations. We calculate the resulting utility and report the average improvement compared to the baseline of using the decision strategy derived when solving the influence diagram with 2 discrete states. Figure 4 presents the average performance improvement when using a discretization of size N to solve the problem. With current formulations, the largest turbine inspection and maintenance instance that can be solved to optimality can use a discretization of size $N = 4$, which on average improves the performance of the decision strategy by 9.2%. In contrast, the largest solvable instance with the proposed formulation uses $N = 6$ discrete states, which results in an improvement of 11.2%, which is 2 percentage points larger compared to using a discretization of size $N = 4$. This example demonstrates that the developed formulations can be leveraged to find decision strategies that outperform the decision strategies found with existing formulations.

CRediT authorship contribution statement

Topias Terho: Investigation, Methodology, Software, Formal analysis, Writing – original draft, Writing – review & editing. **Fabricio Oliveira:** Project administration, Supervision, Funding acquisition, Writing – original draft, Writing

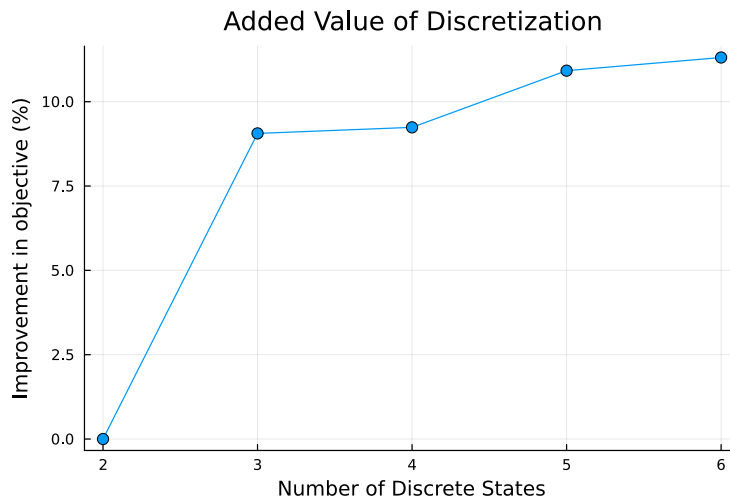


Figure 4: Average relative improvement of optimal decision strategies solved by using a discretization of specific size when compared to a model solved when using 2 discrete states.

– review & editing. **Ahti Salo:** Supervision, Funding acquisition, Writing – original draft, Writing – review & editing. **Pedro Munari:** Methodology, Writing – original draft.

References

de la Barra, J., Salo, A., Pourakbari-Kasmaei, M., 2025. Choosing portfolios of reinforcement actions for distribution grids based on partial information. *Reliability Engineering & System Safety* , 111729.

Basnet, S., BahooToroody, A., Montewka, J., Chaal, M., Banda, O.A.V., 2023. Selecting cost-effective risk control option for advanced maritime operations; integration of stpa-bn-influence diagram. *Ocean Engineering* 280, 114631.

Beuzen, T., Marshall, L., Splinter, K.D., 2018. A comparison of methods for discretizing continuous variables in bayesian networks. *Environmental Modelling & Software* 108, 61–66.

Bielza, C., Gomez, M., Shenoy, P.P., 2010. Modeling challenges with influence diagrams: Constructing probability and utility models. *Decision Support Systems* 49, 354–364.

Borgonovo, E., Tonoli, F., 2014. Decision-network polynomials and the sensitivity of decision-support models. *European Journal of Operational Research* 239, 490–503.

Charnes, A., Cooper, W.W., 1959. Chance-constrained programming. *Management Science* 6, 73–79.

Charnes, J.M., Shenoy, P.P., 2004. Multistage Monte Carlo method for solving influence diagrams using local computation. *Management Science* 50, 405–418.

Cobb, B.R., 2007. Influence diagrams with continuous decision variables and non-gaussian uncertainties. *Decision Analysis* 4, 136–155.

Cobb, B.R., 2021. Statistical process control for the number of defectives with limited memory. *Decision Analysis* 18, 203–217.

Cobb, B.R., Shenoy, P.P., 2008. Decision making with hybrid influence diagrams using mixtures of truncated exponentials. *European Journal of Operational Research* 186, 261–275.

Contasti, A.L., Firth, A.G., Baker, B.H., Brooks, J.P., Locke, M.A., Morin, D.J., 2023. Balancing tradeoffs in climate-smart agriculture: Will selling carbon credits offset potential losses in the net yield income of small-scale soybean (*Glycine max* L.) producers in the mid-southern United States? *Decision Analysis* 20, 252–275.

Falconer, J.R., Frank, E., Polaschek, D.L., Joshi, C., 2024. Eliciting informative priors by modeling expert decision making. *Decision Analysis* 21, 77–90.

French, S., 2024. Whose judgement? Reflections on elicitation in bayesian analysis. *Decision Analysis* 21, 143–159.

González-Ortega, J., Insua, D.R., Cano, J., 2019. Adversarial risk analysis for bi-agent influence diagrams: An algorithmic approach. *European Journal of Operational Research* 273, 1085–1096.

Gu, W., Qiu, J., Hu, J., Tang, X., 2024. A Bayesian decision network-based pre-disaster mitigation model for earthquake-induced cascading events to balance costs and benefits on a limited budget. *Computers & Industrial Engineering* 191, 110161.

Gurobi Optimization, LLC, 2022. Gurobi optimizer reference manual. URL: <https://www.gurobi.com>.

Hankimaa, H., Herrala, O., Oliveira, F., de Balsch, J.T., 2023. Solving influence diagrams via efficient mixed-integer programming formulations and heuristics. arXiv preprint arXiv:2307.13299 .

Hansen, E.A., 2021. An integrated approach to solving influence diagrams and finite-horizon partially observable decision processes. *Artificial Intelligence* 294, 103431.

Herrala, O., Terho, T., Oliveira, F., 2025. Risk-averse decision strategies for influence diagrams using rooted junction trees. *Operations Research Letters* , 107308.

Howard, R.A., Matheson, J.E., 2005a. Influence diagram retrospective. *Decision Analysis* 2, 144–147.

Howard, R.A., Matheson, J.E., 2005b. Influence diagrams. *Decision Analysis* 2, 127–143.

Keating, L.M., Randall, L., Stanton, R., McCormack, C., Lucid, M., Seaborn, T., Converse, S.J., Canessa, S., Moehrenschlager, A., 2023. Using decision analysis to determine the feasibility of a conservation translocation. *Decision Analysis* 20, 295–310.

Khakzad, N., 2021. Optimal firefighting to prevent domino effects: Methodologies based on dynamic influence diagram and mathematical programming. *Reliability Engineering & System Safety* 212, 107577.

Khosravi-Farmad, M., Ghaem-Bafghi, A., 2020. Bayesian decision network-based security risk management framework. *Journal of Network and Systems Management* 28, 1794–1819.

Lauritzen, S.L., Nilsson, D., 2001. Representing and solving decision problems with limited information. *Management Science* 47, 1235–1251.

Li, X., Liu, Y., Chen, G., Abbassi, R., 2024. Dynamic risk-based methodology for economic life assessment of aging subsea pipelines. *Ocean Engineering* 294, 116687.

Lu, Q., Zhang, W., Hughes, W., Bagtzoglou, A.C., 2022. Bayesian decision network-based optimal selection of hardening strategies for power distribution systems. *ASCE-ASME Journal of Risk and Uncertainty in Engineering Systems, Part A: Civil Engineering* 8, 04022038.

Lubin, M., Dowson, O., Dias Garcia, J., Huchette, J., Legat, B., Vielma, J.P., 2023. JuMP 1.0: Recent improvements to a modeling language for mathematical optimization. *Mathematical Programming Computation* 15, 581–589. doi:10.1007/s12532-023-00239-3.

Mancuso, A., Compare, M., Salo, A., Zio, E., 2021. Optimal prognostics and health management-driven inspection and maintenance strategies for industrial systems. *Reliability Engineering & System Safety* 210, 107536.

Mauá, D.D., de Campos, C.P., Zaffalon, M., 2012. Solving limited memory influence diagrams. *Journal of Artificial Intelligence Research* 44, 97–140.

Mauá, D.D., Cozman, F.G., 2016. Fast local search methods for solving limited memory influence diagrams. *International Journal of Approximate Reasoning* 68, 230–245.

Neuvonen, L., Dillon, M., Vilkkumaa, E., Salo, A., Jäntti, M., Heinävaara, S., 2025. Optimizing the Finnish colorectal cancer population screening program with decision programming. *European Journal of Operational Research* 327, 295–308.

Oni, B., Madson, K., MacKenzie, C., 2024. Evaluation of maintenance decisions to optimize navigable inland waterway lock conditions. *Journal of Infrastructure Systems* 30, 04024013.

Parmentier, A., Cohen, V., Leclère, V., Obozinski, G., Salmon, J., 2020. Integer programming on the junction tree polytope for influence diagrams. *INFORMS Journal on Optimization* 2, 209–228.

Penman, T.D., Cirulis, B., Marcot, B.G., 2020. Bayesian decision network modeling for environmental risk management: A wildfire case study. *Journal of Environmental Management* 270, 110735.

Raiffa, H., 1968. *Decision Analysis*. Addison-Wesley.

Rockafellar, R.T., Uryasev, S., et al., 2000. Optimization of conditional value-at-risk. *Journal of Risk* 2, 21–42.

Salo, A., Andelman, J., Oliveira, F., 2022. Decision programming for mixed-integer multi-stage optimization under uncertainty. *European Journal of Operational Research* 299, 550–565.

Shachter, R.D., 1986. Evaluating influence diagrams. *Operations Research* 34, 871–882.

Tatman, J.A., Shachter, R.D., 1990. Dynamic programming and influence diagrams. *IEEE Transactions on Systems, Man, and Cybernetics* 20, 365–379.

Varis, O., Kettunen, J., Sirviö, H., 1990. Bayesian influence diagram approach to complex environmental management including observational design. *Computational Statistics & Data Analysis* 9, 77–91.

Wan, Q., Xu, X., Hunt, K., Zhuang, J., 2022. Stay home or not? Modeling individuals' decisions during the COVID-19 pandemic. *Decision Analysis* 19, 319–336.

Weflen, E., MacKenzie, C.A., Rivero, I.V., 2022. An influence diagram approach to automating lead time estimation in agile Kanban project management. *Expert Systems with Applications* 187, 115866.

Zhang, N.L., Qi, R., Poole, D., 1994. A computational theory of decision networks. *International Journal of Approximate Reasoning* 11, 83–158.